SCIEPublish

Article

Adsorption of Bisphenol A and 2,6-Dichlorophenol in Water Using Magnetic Phosphogypsum Composite Materials

Meng Lu [1,2], Jiangui Jiang [3], Ru-an Chi [1], Junxia Yu [3], Qingbiao Zhao [1,*] and Dezeng Li [2,*]

[1] Hubei Three Gorges Laboratory, No. 1 Mazongling Rd, Xiaoting District, Yichang 443007, China; xzalumeng@163.com (M.L.); rac@wit.edu.cn (R.-a.C.)

[2] School of Chemistry and Molecular Engineering, East China Normal University, Shanghai 200241, China

[3] School of Chemistry and Environmental Engineering, Wuhan Institute of Technology, Wuhan 430079, China; 22309010109@stu.wit.edu.cn (J.J.); yujunxia_1979@163.com (J.Y.)

* Corresponding author. E-mail: 23031701@wit.edu.cn (Q.Z.) lidz@chem.ecnu.edu.cn (D.L.)

Received: 2 November 2024; Accepted: 3 December 2024; Available online: 12 December 2024

ABSTRACT: Phenolic pollutants in water bodies pose a huge threat to human health and environmental safety. In this paper, a hydrophobicity-enhanced magnetic C-SiO_2/MPG composite was prepared by a two-step method to remove bisphenol A (BPA)and 2,6-dichlorophenol (2,6-DCP), typical phenolic trace pollutants in livestock wastewater and natural water bodies. The results of pH gradient experiments showed that C-SiO_2/MPG showed a stable removal effect on BPA in the pH range of 2–11. The adsorption of 2,6-DCP by C-SiO_2/MPG peaked at pH = 2, while the adsorption of 2,6-DCP by C-SiO_2/MPG was severely inhibited under alkaline conditions. The PSO kinetic model and the Langmuir isotherm model can better describe the adsorption process of BPA and 2,6-DCP on C-SiO_2/MPG, indicating that the monolayer chemical adsorption has a rate-controlling step. With the Langmuir equation fitting, the maximum adsorption capacity of C-SiO_2/MPG for BPA and 2,6-DCP at 298 K was calculated to be 561.79 mg/g and 531.91 mg/g, respectively. The results of adsorption thermodynamics indicated that the adsorption of BPA and 2,6-DCP on C-SiO_2/MPG was spontaneous, accompanied by a process of entropy decrease. C-SiO_2/MPG showed good environmental resistance and repeated use stability for BPA and 2,6-DCP in electrolyte ion interference, actual water samples and cycle experiments. Mechanism analysis showed that the adsorption of BPA and 2,6-DCP on C-SiO_2/MPG was mainly controlled by hydrogen bonding and hydrophobic interactions. This study designed an efficient adsorbent for phenolic pollutants that can be used in actual wastewater and broadened the resource utilization of industrial waste phosphogypsm.

Keywords: Phosphogypsum; Magnetic nanoparticles; Hydrophobic alkyl chains; Adsorption; Phenolic pollutants; Water pollution

1. Introduction

The development of industrialization is accompanied by an increase in the amount of persistent pollutants discharged into the environment by various industries. BPA and 2,6-DCP are typical phenolic pollutants in livestock wastewater and natural water bodies [1]. Bisphenol A (4,4′-isopropyldiphenol, BPA) is widely used in the manufacture of plastics, resins, food packaging and coatings. Exposure to this compound produces estrogenic effects in a variety of organisms [2]. 2,6-DCP is listed as a priority pollutant due to its persistence and high toxicity in the environment [3]. Based on environmental protection, treating the ubiquitous phenolic wastewater is an urgent task to effectively protect human health and the safety of natural ecosystems. In a recent study, phosphogypsum was used as an adsorbent to remove phenol from coking wastewater. The study tested phosphogypsum as a phenol adsorbent in actual coking wastewater in static and dynamic modes at an initial phenol concentration of 395 mg/L. The maximum adsorption capacity reached 85 mg/g in intermittent mode and 124 mg/g in column mode [4]. The study showed that phosphogypsum can be effectively used for pretreatment of phenol wastewater before biological treatment. In addition, it has been previously reported in the literature that calcined gypsum was used as an adsorbent to remove phenol from synthetic wastewater with an initial phenol content of about 36 mg/L. The maximum adsorption capacity reached 2.94 mg/g and the purification efficiency was 84.25% [5]. These related reports show that phosphogypsum-based materials

https://doi.org/10.70322/gct.2024.10007

have a certain potential to remove phenolic pollutants. However, original phosphogypsum (PG) lacks affinity for organic matter and exhibits limited adsorption capacity for phenolic pollutants. Modifying PG with inorganic or organic materials to develop new functional PG-based adsorbents is an effective way to overcome this limitation [6]. Inspired by magnetic separation technology, adsorbents modified with superparamagnetic nanoparticles can avoid time-consuming centrifugation or filtration steps to speed up the solid-liquid separation [7]. Studies have shown that the adsorption of phenolic compounds by raw PG is mainly carried out through a physical adsorption mechanism. Compared with widely studied materials such as activated carbon, the adsorption capacity of raw PG for phenolic compounds is very low at 85 mg/g [4]. Modification with cationic surfactants is an effective strategy to improve the adsorbent for removing hydrophobic phenolic pollutants [1,8]. CTAB is one of the effective surfactants commonly used in modifying materials. The addition of CTAB makes the material surface have more negatively charged adsorption sites, which enhances the adsorption of anions [9–12]. The deposition of the surfactant layer for enhancing the hydrophobicity of the magnetic material can be achieved by a sol-gel procedure [6,13,14], in which silica acts as a stabilizer and modifier to suppress the dissolution tendency of the magnetic particles in acidic solutions [6,8,15].

In this study, a two-step method was used to prepare a magnetic C-SiO_2/MPG composite with improved hydrophobicity. First, a magnetic PG (MPG) composite was prepared using a simple coprecipitation method, followed by the deposition of CTAB on the MPG surface via a sol-gel process. This inorganic-organic hybrid material has both the magnetic properties of Fe_3O_4 nanoparticles and the hydrophobicity of C_{16} alkyl chains. It can be used as an adsorbent material for the effective removal of phenols in water. In this paper, the removal capability of C-SiO_2/MPG for pollutants BPA and 2,6-DCP was comprehensively evaluated by investigating the key factors affecting the adsorption process, and the potential mechanism of BPA and 2,6-DCP adsorption was further explored. The study of the adsorption of hydrophobic organic pollutants BPA and 2,6-DCP in water by PG and modified C-SiO_2/MPG is beneficial to the environment in terms of water treatment, solid waste management and energy production.

2. Materials and Methods

2.1. Experimental Reagents

BPA ($C_{15}H_{16}O_2$, >98%), $FeCl_3 \cdot 6H_2O$ (99%), $FeCl_2 \cdot 4H_2O$ (98%), CTAB ($C_{19}H_{42}BrN$, >98%), C_3H_8O (>99.7%), NaOH (96%) were purchased from Titan (Shanghai, China). 2,6-DCP ($C_6H_4Cl_2O$ 99%) was supplied by Boer (Shanghai, China). TEOS (>98%), C_2H_6O (>99.7%), HCl (38%) were purchased from Sinopharm Chemical Reagent Co., Ltd. (Shanghai, China).

2.2. Preparation of MPG and C-SiO_2/MPG Composites

The magnetic PG (MPG) composite was synthesized using the coprecipitation method. 75 mL of DIW was heated to 85 °C under N_2 atmosphere, and then 2.5 g of PG and Fe^{3+} and Fe^{2+} in a molar ratio of 2:1 were added [16]. After vigorous stirring for 1 h, the suspension was collected by an external magnet and washed with DIW and ethanol. The obtained MPG was dried in an oven at 60 °C. C-SiO_2/MPG was synthesized by improving the previously reported sol-gel method [6]. That is, MPG was dispersed in 15 mL of DIW to form a suspension, and then a solution containing 15 g of TEOS, 1.5 g of CTAB and 5 mL of 2-propanol was slowly added thereto, and the pH value of the mixture was adjusted to 10. After stirring, a gel was formed, and C-SiO_2/MPG was collected under an external magnet and washed with ethanol and DIW several times. Finally, the composite was dried at room temperature. Using the same method, MPG modified with only CTAB (C/MPG), only TEOS (SiO_2/MPG), and the amount of TEOS unchanged but the amount of CTAB changed were prepared.

2.3. Testing and Characterization

Scanning electron microscopy (SEM) images were recorded with a Hitachi SU8220 (Tokyo, Japan) instrument. Powder X-ray diffraction (XRD) patterns were obtained with a Rigaku Corporation Smartlab SEX (Akishima, Japan) instrument. Fouri-er-transform infrared (FT-IR) spectra of samples were collected on a Nicolet iS50 FT-IR spectrometer from Thermo Fisher Scientific Inc. (Waltham, MA, USA) A thermal analyzer (DSC3+) was applied to perform thermogravimetric analysis (TGA) of the materials. Brunauer-Emmett-Teller (BET) surface areas and pore volumes of MPG and C-SiO_2/MPG were determined by N_2 adsorption-desorption data with a gas adsorption analyzer (Autosorb-IQ, Dresden, Germany). The absorbance of BPA and 2,6-DCP solution was measured by Ultraviolet-visible spectrophotometer (UV-8000, Metash, Shanghai, China). The surface chemical compositions of C-SiO_2/MPG

composite materials before and after adsorption of BPA and 2,6-DCP were analyzed by X-ray photoelectron spectroscopy (XPS, AXIS SUPRA). The pH meter (pHS-3C, Rex Electric Chemical, Shanghai, China) was used to determine the pH of MPG and C-SiO_2/MPG. The zeta potential of MPG and C-SiO_2/MPG was measured in the pH range of 2–11 using a zeta potentiometer (Nano ZS3600).

2.4. Analysis Conditions of Pollutants and Standard Curves

The prepared 100 mg/L BPA and 2,6-DCP standard stock solutions were diluted to prepare standard solutions with concentrations of 1–5 mg/L. Absorbance was measured at wavelengths of 274 nm and 281 nm, and standard absorbance curves for the two phenolic solutions were plotted[17,18]. As shown in Figure 1, the fitting equations were used to calculate the concentrations of BPA and 2,6-DCP.

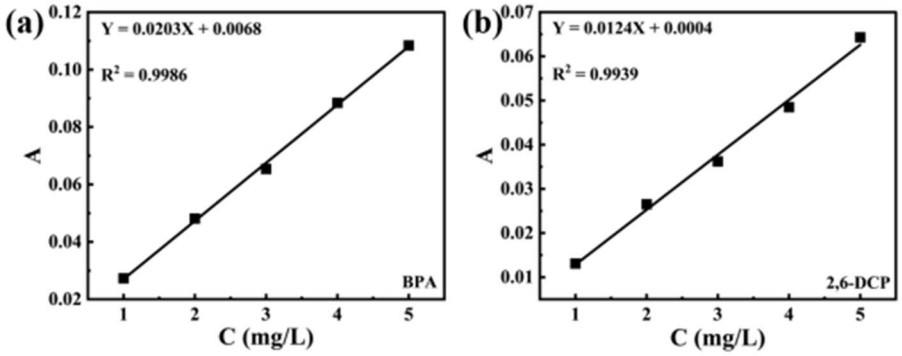

Figure 1. Standard absorbance curves of (**a**) BPA and (**b**) 2,6-DCP.

2.5. Adsorption of BPA and 2,6-DCP on C-SiO_2/MPG

2.5.1. Batch Adsorption Experiments

The stock solution of BPA (200 mg/L) was dissolved in a mixed solvent of deionized water and ethanol (9:1, *v*/*v*), and the stock solution was further diluted with deionized water to obtain the desired concentration. The stock solution of 2,6-DCP was directly prepared with deionized water as the solvent. The effects of various factors on the adsorption of BPA and 2,6-DCP by C-SiO_2/MPG were determined by conducting experiments at different adsorbent doses (2.4–14.4 mg), pH (2–11), contact times (10–130 min), initial phenolic concentrations (5–160 mg/L), and three temperatures (298–318 K). After a fixed adsorption time, the solution was separated from the adsorbent C-SiO_2/MPG using an external magnetic field, and the concentrations of residual BPA and 2,6-DCP in the separated solution were determined by UV-visible spectrophotometry. Each experiment was repeated at least three times to determine the reproducibility and validity of the data. Equations (1)–(3) give the expressions for the adsorption amount and adsorption removal rate calculated using the mass balance method.

$$\%RE = \frac{C_0 - C_t}{C_0} \times 100\% \quad (1)$$

$$Q_t = \frac{C_0 - C_t}{m} \times V \quad (2)$$

$$Q_e = \frac{C_0 - C_e}{m} \times V \quad (3)$$

In the above formula, C_0 (mg/L), C_t (mg/L) and C_e (mg/L) represent the concentrations of phenolic pollutants at the initial, specified time and equilibrium state, respectively. V (L) is the volume in the batch adsorption experiment, and m (g) is the amount of adsorbent used.

2.5.2. Adsorption Kinetics Studies

The kinetic adsorption experimental data were obtained under the experimental conditions of temperature of 298 K, time of 10–130 min, and phenol concentrations of 20, 50, and 100 mg/L. The pH of the BPA solution was not adjusted, the pH of the 2,6-DCP solution needed to be adjusted to 2, and the dosage of C-SiO_2/MPG was 7.2 mg.

2.5.3. Adsorption Isotherm Studies

The adsorption isotherms at three temperatures were conducted in aqueous solutions of BPA and 2,6-DCP with concentrations ranging from 5 to 160 mg/L. The pH of the BPA solution was not adjusted, while the pH of the 2,6-DCP solution needed to be adjusted to 2. The dosage of C-SiO_2/MPG was 7.2 mg, and the contact time was 90 min.

2.5.4. Adsorption Thermodynamics Study

In the experiment to explore the effect of temperature on the adsorption process, the pH of the BPA solution was not adjusted, the pH of the 2,6-DCP solution was adjusted to 2, the dosage of C-SiO_2/MPG was 7.2 mg, and the contact time was 90 min.

2.6. Effect of Background Electrolyte and Humic Acid

The effects of typical inorganic ions and organic matter on the adsorption of BPA and 2,6-DCP were investigated. Electrolyte ions and HA were introduced into the solution. Four different concentrations (0, 0.01, 0.1, and 1 mol/L) were set to study the effects of cations and anions on the adsorption of phenolic pollutants. Sodium salts were used when studying the effects of different anions (Cl^-, NO_3^-, SO_4^{2-}, HPO_4^{2-}, and PO_4^{3-}); chloride salts were used when studying the effects of different cations (Na^+, K^+, Ca^{2+}, and Al^{3+}). When studying the effect of HA on adsorption, the concentrations of BPA and 2,6-DCP were fixed at 100 mg/L, and the concentration of HA was changed from 50 mg/L to 250 mg/L.

2.7. Adsorption Performance of C-SiO_2/MPG in Real Water Samples

To investigate the potential of this method, C-SiO_2/MPG was applied to remove BPA and 2,6-DCP from real water samples. Four concentration levels (20, 40, 60, and 80 mg/L) of BPA and 2,6-DCP were prepared in all DIW, TP, and RW water samples, and the experiments were conducted under optimized parameters.

2.8. Regeneration Experiment of C-SiO_2/MPG

C-SiO_2/MPG was regenerated by washing with ethanol and subjected to six consecutive adsorption-desorption cycles in 100 mg/L BPA and 2,6-DCP solutions under optimized parameters to determine the reusability of C-SiO_2/MPG in industrial wastewater treatment applications.

3. Results and Discussion

3.1. Characterization of Materials

The surface morphology of MPG and C-SiO_2/MPG were characterized with SEM (Figure 2). Compared with PG, Figure 2a,b shows the presence of small spherical aggregates on the surface of PG, which is due to the co-precipitation of magnetic nano-Fe_3O_4 on the surface of PG, which makes MPG respond strongly to the magnetic field [19]. As shown in the SEM images of Figure 2c,d, the C-SiO_2/MPG particles have an irregular morphology, and the observed spheres can be attributed to the presence of hydrophobic C_{16} silicone prepared by TEOS and CTAB [6].

EDS spectrum confirmed that MPG was formed by co-precipitation [16]. Compared with PG, Fe and O peaks appeared in MPG. The main elements in the MPG composite material were Fe (6.13%), O (76.56%), Ca (7.99%) and S (9.32%) (Figure 3a). The element distribution diagram in Figure 3b shows that the Fe_3O_4 particles are evenly coated on the surface of PG, which also confirms the presence of Fe, O, Ca, and S. Figure 3c shows that in addition to the Fe, O, Ca, and S signals present in MPG, the presence of Si, N and C element signals confirm the formation of C-SiO_2/MPG. The changes in elemental composition and signal intensity are due to the incorporation of TEOS during the sol-gel process, which confirms the presence of C_{16} alkyl chains and organic SiO_2 on C-SiO_2/MPG [17]. The elemental map in Figure 3d also confirms the presence of Si, N and C, which is consistent with the energy spectrum results.

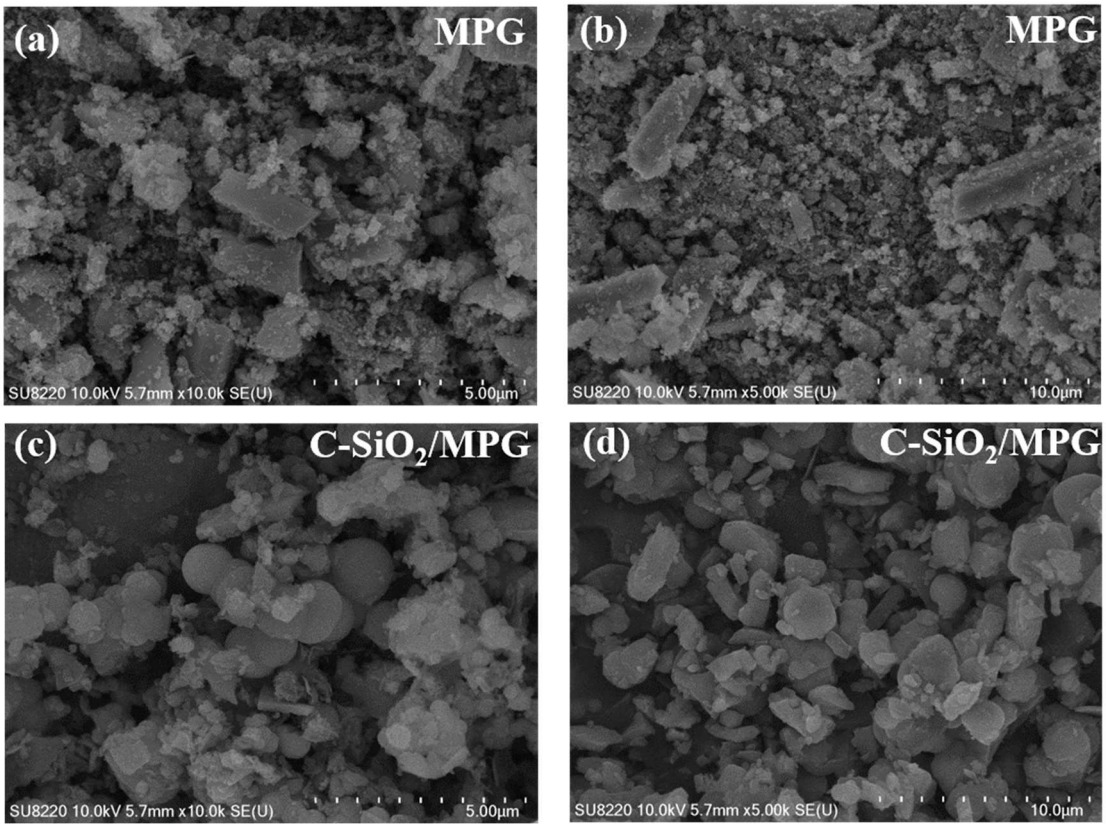

Figure 2. Morphologies of (**a**,**b**) MPG and (**c**,**d**) C-SiO_2/MPG.

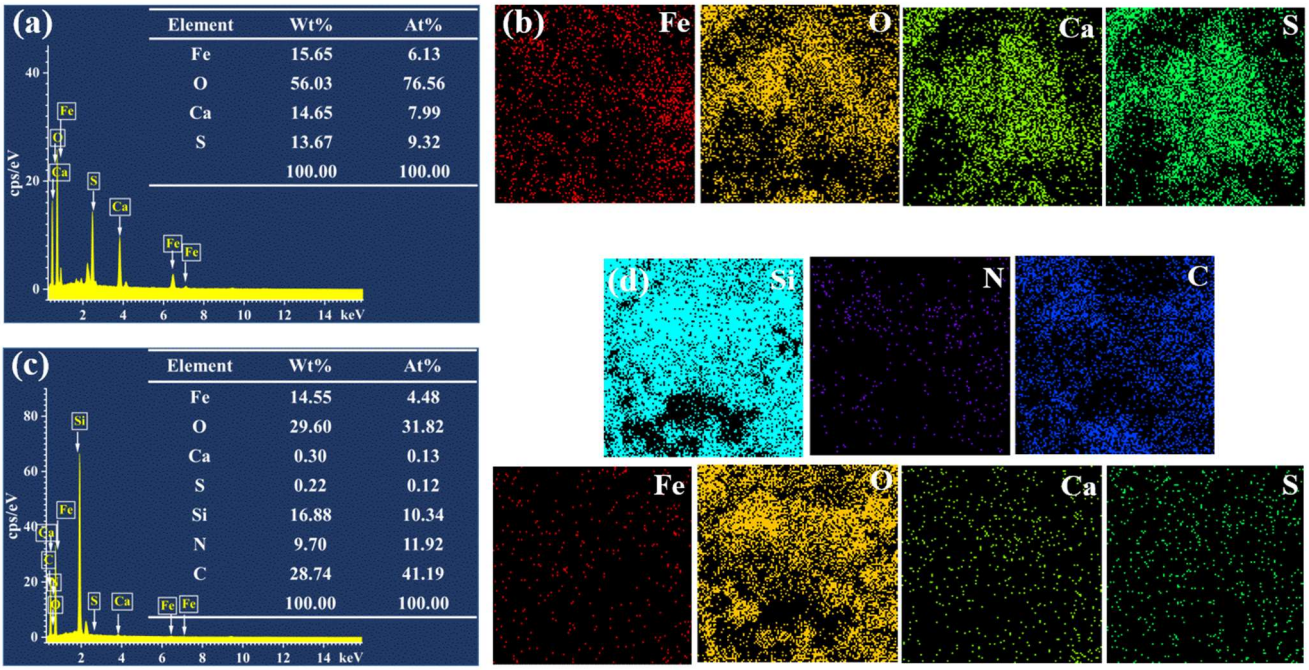

Figure 3. (**a**) Energy spectra of MPG and (**c**) C-SiO_2/MPG; (**b**) Element distribution of MPG and (**d**) C-SiO_2/MPG.

Figure 4a,b shows the SEM images of C-SiO_2/MPG after adsorption of BPA and 2,6-DCP. In comparison, the surface morphology has not changed significantly. The energy spectrum analysis of Figure 4c,d shows that the content of C and O elements in C-SiO_2/MPG increases after adsorption of BPA and 2,6-DCP, and the presence of Cl element is attributed to 2,6-DCP. These characterization results verify the adsorption of BPA and 2,6-DCP on the surface of C-SiO_2/MPG [20].

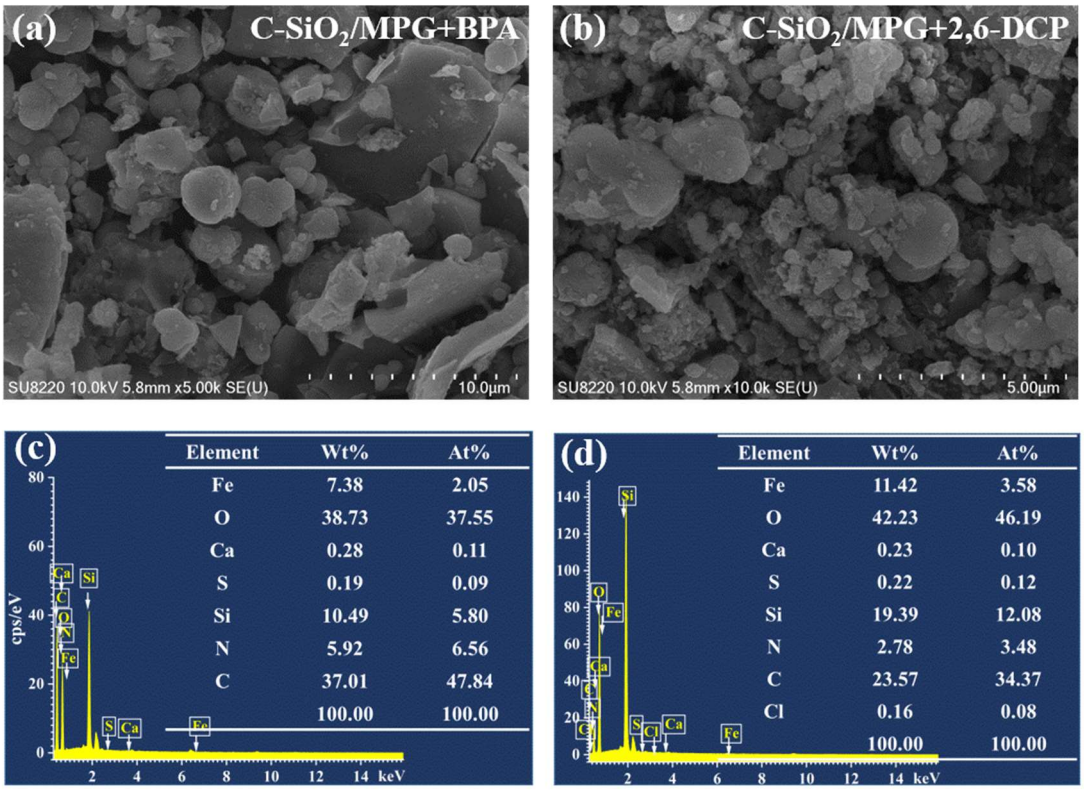

Figure 4. Morphology of C-SiO_2/MPG after adsorption of (**a**) BPA and (**b**) 2,6-DCP; Energy spectrum of C-SiO_2/MPG after adsorption of (**c**) BPA and (**d**) 2,6-DCP.

The crystal structures of MPG and C-SiO_2/MPG composites were characterized by XRD, as shown in Figure 5a,b. In the 2θ range of 25–70°, a series of characteristic peaks at 30.41°, 35.56°, 43.54°, 57.25° and 62.73° match well with the (220), (311), (400), (511) and (440) planes of the typical cubic inverse spinel structure (PDF#19-0629) [21]. After magnetization treatment, the initial XRD characteristic peaks of PG can still be observed, indicating that the co-precipitation of Fe_3O_4 has no obvious effect on the crystal structure of PG. In addition, the characteristic diffraction peak belonging to the (311) plane of Fe_3O_4 observed at 35.75° for the MPG sample confirms the presence of Fe_3O_4 and the successful synthesis of MPG. After SiO_2 surface coating, a broad and weak peak was observed at 2θ = 20–30° for the C-SiO_2/MPG sample, which is the characteristic peak of amorphous SiO_2 [22]. The test results in Figure 5b show that during the SiO_2 coating process, MPG maintains its original crystal structure characteristics. However, the intensity of the four main characteristic peaks related to PG is reduced, which is attributed to the dense organic SiO_2 coating in C-SiO_2/MPG [23]. Additionally, the weakening of the diffraction peak intensity indicates the adhesion of the surfactant CTAB to the C-SiO_2/MPG surface.

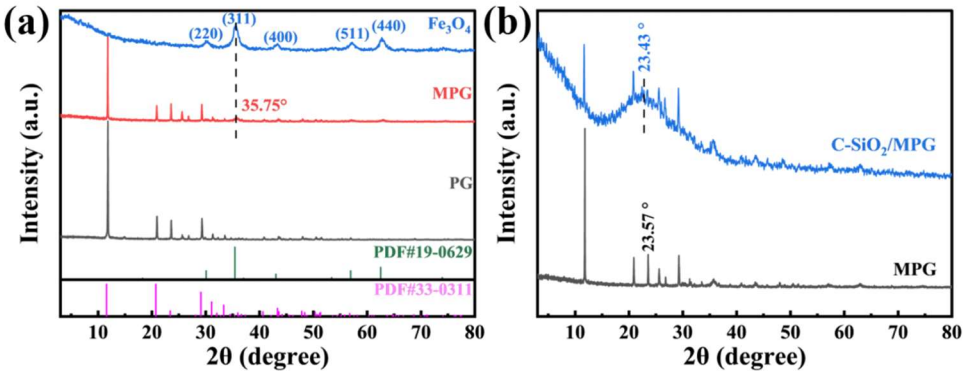

Figure 5. XRD spectra of (**a**) PG, MPG and Fe_3O_4, (**b**) C-SiO_2/MPG.

FT-IR spectroscopy was used to analyze the functional groups in the composite materials MPG and C-SiO_2/MPG, as shown in Figure 6a. Compared with PG, MPG shows absorption bonds corresponding to the stretching vibrations of Fe^{2+}-O^{2-} and Fe^{3+}-O^{2-} groups of Fe_3O_4 at 599 and 445 cm^{-1}, which indicates the successful deposition of magnetic particles on the PG surface [24]. Several new characteristic peaks appeared when CTAB formed a composite with MPG using the sol-gel process. The 2928 and 2854 cm^{-1} bands correspond to the C-H symmetric and antisymmetric stretching vibration peaks of -CH_3 and -CH_2 in the CTAB alkyl chain, 1468 cm^{-1} represents the bending vibration of C-H, and 962 cm^{-1} represents the out-of-plane bending vibration peak of C-N. The appearance of the above peaks indicates the presence of CTAB in C-SiO_2/MPG [7,10]. The stretching vibrations of Si-O-Si and Si-OH are assigned to the strong peaks near 1088 cm^{-1}, the band at 470 cm^{-1} is the bending vibration of O-Si-O bonds, and the broadband observed near 3462 cm^{-1} is due to the -OH stretching frequency of the silanol group [15,25].

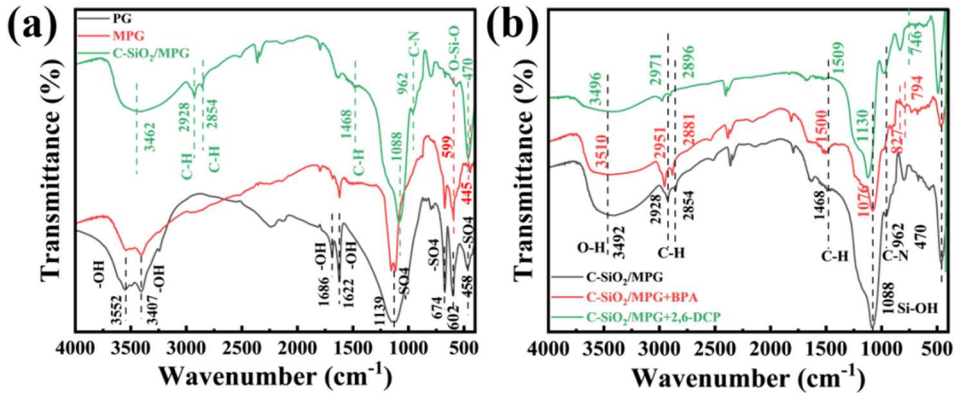

Figure 6. FT-IR spectra of (**a**) PG, MG, and C-SiO_2/MPG and (**b**) C-SiO_2/MPG adsorbing BPA and 2,6-DCP.

As shown in Figure 6b, the spectrum of C-SiO_2/MPG after adsorption of phenols, the characteristic peaks of BPA were observed at 827 cm^{-1} and 794 cm^{-1}, corresponding to the γ-CH vibration on the 1,4 disubstituted aromatic ring of BPA and the bending vibration of C-H on the benzene ring. The characteristic peak of -OH was weakened after adsorption of BPA [10,15]. The main peak shifts and peak intensity reductions in the C-SiO_2/MPG spectrum were observed at 3492 cm^{-1}, 2928 cm^{-1}, 2854 cm^{-1}, 1468 cm^{-1} and 1088 cm^{-1}, corresponding to -OH, C-H in -CH_3, C-H in -CH_2, Si-O-Si and Si-OH, respectively. The reduction in peak shifts and intensities further confirmed that the above groups were involved in the adsorption of BPA. Therefore, the -OH and alkyl chains in C-SiO_2/MPG can promote the adsorption and removal of BPA through hydrogen bonding and hydrophobic interactions [26]. It can also be found from the figure that the absorption peaks of -OH and C-H in C-SiO_2/MPG have different degrees of shift after the adsorption of 2,6-DCP, which also indicates that the functional groups on its surface participate in the adsorption process. The weak characteristic peak centered at 746 cm^{-1} belongs to the C-Cl band of 2,6-DCP. The characteristic peak at 1088 cm^{-1} shifts to 1130 cm^{-1} after adsorption, corresponding to the phenolic group with ortho and para chlorine atoms of 2,6-DCP[27]. The -OH bond absorption peak of C-SiO_2/MPG at 3492 cm^{-1} shifts and is broadened after adsorption, indicating that hydrogen bonding is involved in the adsorption process of 2,6-DCP by C-SiO_2/MPG.

The thermal stability curves of TEOS and CTAB modified PG were studied, as shown in Figure 7. In Figure 7a, the weight losses of MPG, C/MPG and SiO_2/MPG in the test temperature range are 17.1%, 8.5% and 16.4%, respectively. A comparison of C-SiO_2/MPG modified with different amounts of CTAB shows that both exhibit the same thermal decomposition trend. In this temperature range, the organic silanol (SiOH) group is dehydroxylated from the surface of C-SiO_2/MPG [25]. However, with the increase of CTAB addition, the thermal stability of C-SiO_2/MPG decreased, and the weight loss rates of C-SiO_2/MPG (2.5 g CTAB), C-SiO_2/MPG (1.5 g CTAB) and C-SiO_2/MPG (0.5 g CTAB) were 32.6%, 26.2% and 18.9%, respectively. The subsequent batch adsorption experiment used hydrophobic magnetic C-SiO_2/MPG with the addition of 1.5 g CTAB.

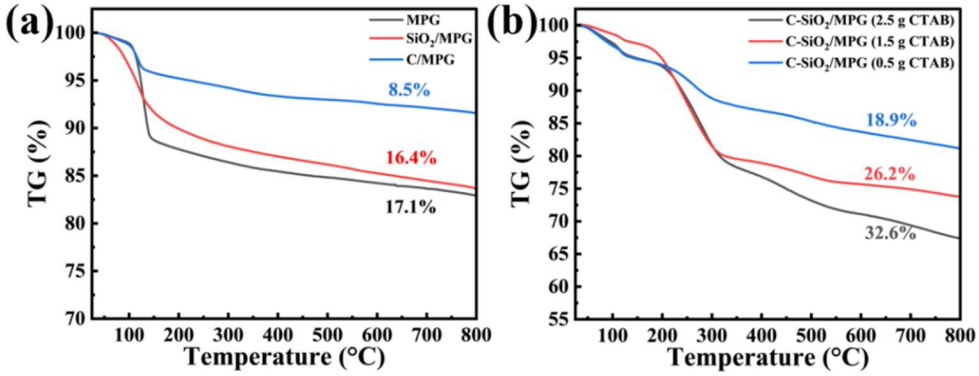

Figure 7. TGA curves of (**a**) MPG, C/MPG and SiO_2/MPG and (**b**) C-SiO_2/MPG with different CTAB addition amounts.

The BET analysis results of MPG and C-SiO_2/MPG are shown in Figure 8. The results show that MPG exhibits a type IV isotherm, in which the hysteresis loop belongs to the H_3 type [7]. The BET specific surface area of PG is 25.5 m^2/g, and the attachment of Fe_3O_4 nanoparticle on PG increases the BET specific surface area of MPG to 63.1 m^2/g [28]. The isotherm of C-SiO_2/MPG is similar to that of MPG, with an H_3 type hysteresis loop and a specific surface area of 68.8 m^2/g. In comparison, Nilgün Balkaya showed that the specific surface area of lime-pretreated phosphogypsum was only 6.228 m^2/g [29]. Similarly, the results of Lina Zhao et al. showed that the specific surface area of phosphogypsum was 20.41 m^2/g. In comparison, the specific surface area of SDBS@PG modified with sodium dodecylbenzene sulfonate (SDBS) was only 16.58 m^2/g [30]. In this work, the specific surface area increased from 25.52 m2/g to 68.8 m^2/g after modifying PG. This improvement increased the contact area between the pollutant and the adsorbent, improving the adsorption effect. It is noteworthy that magnetic nanoparticles can be successfully supported in the PG matrix and provide magnetic properties to the functionalized PG-based adsorbent.

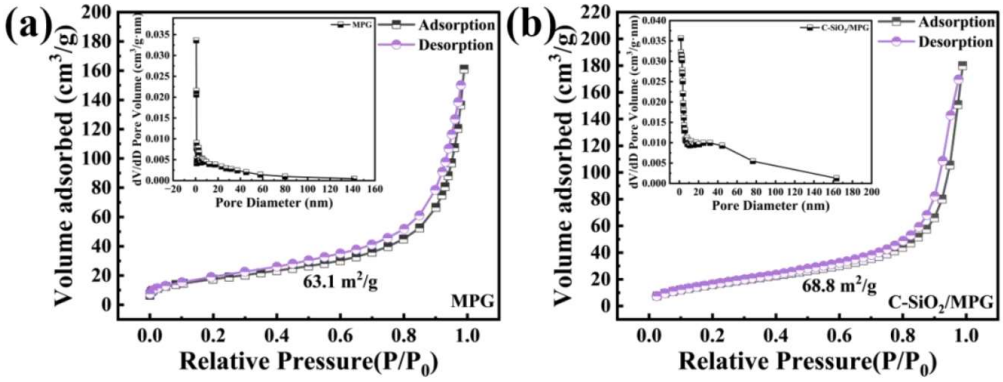

Figure 8. N_2 adsorption-desorption curves and pore size distribution of (**a**) MPG and (**b**) C-SiO_2/MPG.

As shown in Figure 9, the chemical composition of PG, MPG, and C-SiO_2/MPG was analyzed using XPS. Figure 9a shows that the MPG sample mainly contains four elements: Fe, O, Ca, and S. This result is consistent with the previous XRD results [31]. The two obvious peaks of MPG at 532.03 eV and 711.17 eV belong to the surface O and Fe elements respectively. In contrast, the peak of MPG for O 1s is slightly stronger than that of PG, which is attributed to the presence of Fe_3O_4 (lattice oxygen in metal oxides, O^{2-}) [28]. N and Si elements appear in the survey XPS spectrum of C-SiO_2/MPG, which is attributed to the composite of CTAB and TEOS on the MPG surface. Figure 9b shows the XPS spectra of C-SiO_2/MPG after adsorption of BPA and 2,6-DCP. The changes in C and O elements and the appearance of Cl at 200.66 eV prove the adsorption of BPA and 2,6-DCP, which is consistent with the above EDS results [18]. After adsorption of BPA and 2,6-DCP, the main peak of N 1s moved to 402.86 eV and 402.75 eV, respectively, and the content of N element also decreased. Figure 9c shows the spectrum of Fe 2p, where the four peaks at 710.24, 711.90, 723.43 and 725.33 eV correspond to Fe^{2+} 2p3/2, Fe^{3+} 2p3/2, Fe^{2+} 2p1/2 and Fe^{3+} 2p1/2, respectively. The presence of positive trivalent and positive divalent Fe further proves that Fe_3O_4 exists in MPG in a co-precipitated manner [7,31]. As shown in Figure 9d, the single peak centered at 103.09 eV in C-SiO_2/MPG is attributed to the O-Si-

O network bond structure of SiO_2 [32]. Before adsorption, the high-resolution N 1s peak in C-SiO_2/MPG was deconvoluted into two components at 399.89 and 402.64 eV, which was attributed to the presence of C-NH_2 and -NH_3^+ [7].

As shown in Figure 9e, after the adsorption of BPA and 2,6-DCP, the N 1s peak diagram showed changes in binding energy position and intensity, indicating that there may be hydrogen bonds between the amino N atoms in C-SiO_2/MPG and the phenolic hydroxyl hydrogen atoms in BPA and 2,6-DCP [7]. From Figure 9f, three peaks of 284.75, 286.43 and 288.97 eV in the C 1s spectrum can be fitted, which are attributed to C-C, C-N and O-C=O bonds, respectively. They mainly come from the CTAB and TEOS components doped on MPG [31]. The peaks corresponding to the C-C and C-N bonds in C-SiO_2/MPG shifted after the adsorption of BPA and 2,6-DCP, while the peak of O-C=O almost disappeared after the adsorption of BPA and shifted significantly after the adsorption of 2,6-DCP. This is because part of BPA and 2,6-DCP were adsorbed on the hydrophobic functional groups of C-SiO_2/MPG [33]. This further supports the results of FT-IR analysis.

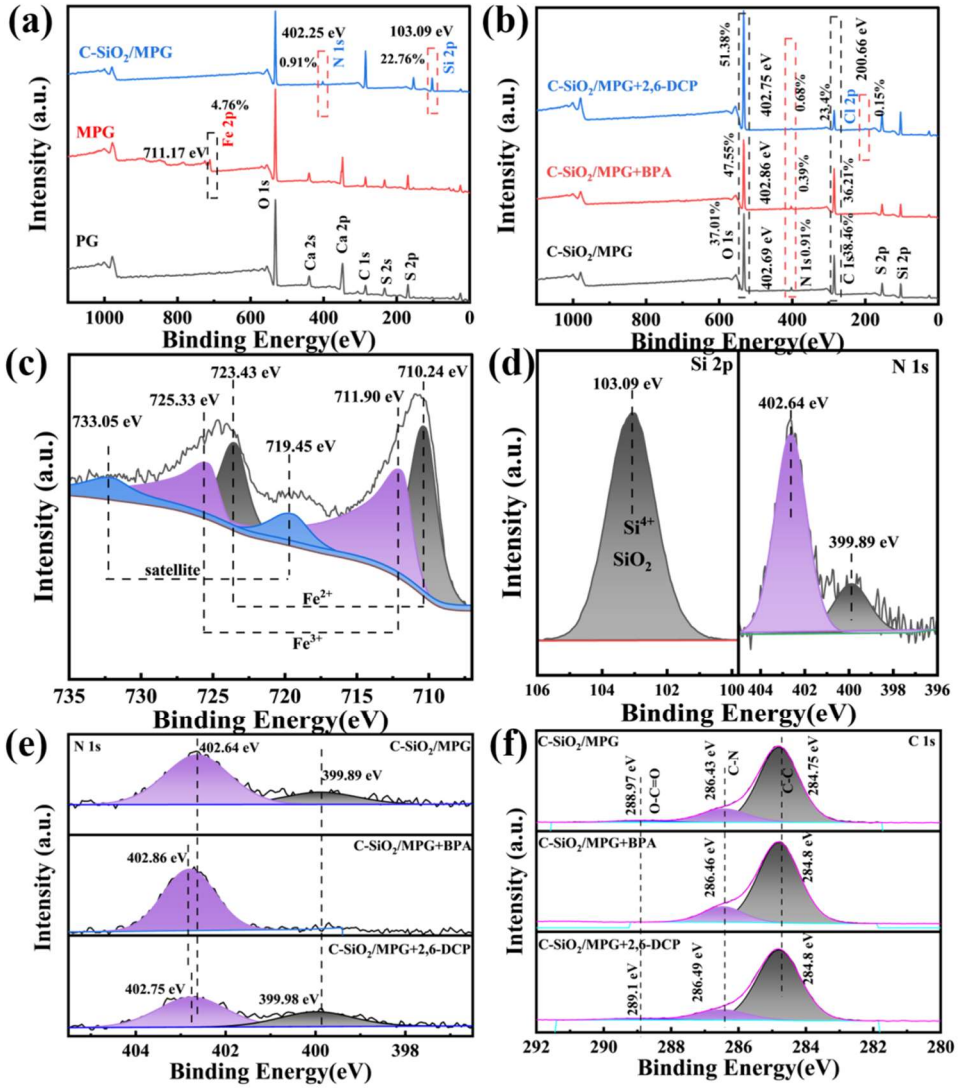

Figure 9. (**a**) XPS spectra of PG, MPG and C-SiO_2/MPG and (**b**) BPA and 2,6-DCP adsorbed on C-SiO_2/MPG; (**c**) XPS spectra of Fe 2p in MPG and (**d**) Si 2p and N 1s in C-SiO_2/MPG; (**e**) N 1s and (**f**) C 1s peak after adsorption on C-SiO_2/MPG.

As shown in Figure 10a, the pH_{pzc} of MPG is 2.9, and the pH_{pzc} of C-SiO_2/MPG (0.5 g CTAB) is 4.3. The surface charges of MPG and C-SiO_2/MPG (0.5 g CTAB) become negative at pH > 5.0, and in the range of 5–11, the charge value of C-SiO_2/MPG (0.5 g CTAB) is more negative than that of MPG, which may be attributed to the ionization of -OH on the surface of organic SiO_2 in C-SiO_2/MPG (0.5 g CTAB). In C-SiO_2/MPG (1.5 g CTAB), due to electrostatic attraction, more alkylammonium cations (CTA+) in CTAB are adsorbed on the surface of C-SiO_2/MPG, which increases its zeta potential in the pH range of 2–11 [25]. At the same time, the absolute value of the zeta potential of C-SiO_2/MPG (1.5 g CTAB) in neutral water is 13.8 mV, which is higher than that of MPG (2.5 mV) and C-SiO_2/MPG (0.5 g CTAB) (10.2 mV).

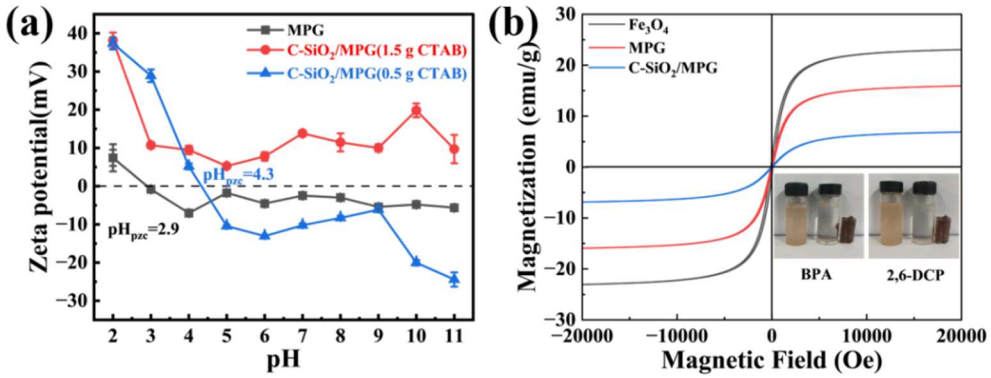

Figure 10. (**a**) Zeta potential values of MPG and C-SiO_2/MPG as a function of pH; (**b**) Hysteresis loops of Fe_3O_4, MPG and C-SiO_2/MPG at room temperature.

The hysteresis loops of Fe_3O_4, MPG and C-SiO_2/MPG at room temperature were recorded to illustrate the changes in the magnetic properties of the materials before and after modification, as shown in Figure 10b. The saturation magnetization of MPG is 31.8 emu/g, which is lower than the magnetic saturation value of Fe_3O_4 (46.1 emu/g), which is mainly due to the presence of PG and the agglomeration of Fe_3O_4 particles in MPG [31]. The modification of MPG surface with TEOS and CTAB further reduces its saturation magnetization to 13.7 emu/g, which is mainly due to the introduction of non-magnetic SiO_2 on the surface of MPG particles. The inset results in Figure 4b show that the prepared C-SiO_2/MPG composite material has sufficient magnetic saturation value under an external magnetic field, which is convenient for rapid separation and recovery from the solvent using an external magnetic field [23].

3.2. Adsorption Comparison before and after Modification

In order to ensure the high adsorption performance of the prepared adsorbent for hydrophobic BPA and 2,6-DCP, the adsorption of BPA and 2,6-DCP by PG, MPG, C/MPG, SiO_2/MPG and C-SiO_2/MPG under the same experimental conditions was compared. As shown in Figure 11, the adsorption capacity of MPG for BPA and 2,6-DCP is slightly lower than that of PG, which may be due to the presence of magnetic nanoparticles leading to the overlap or aggregation of adsorption sites in MPG [34]. C/MPG and SiO_2/MPG have higher adsorption capacity than PG and MPG. The improvement of their adsorption performance can be attributed to the enhanced affinity of BPA and 2,6-DCP for the hydrophobic alkyl functional groups in C-SiO_2/MPG composites [35], and the hydrogen bonding between the -OH functional groups on the silanol surface and the phenolic hydroxyl groups in BPA and 2,6-DCP [26]. The above results show that the high adsorption capacity of the hydrophobic magnetic composite C-SiO_2/MPG for BPA and 2,6-DCP is attributed to the hydrophobic and hydrogen bonding interactions.

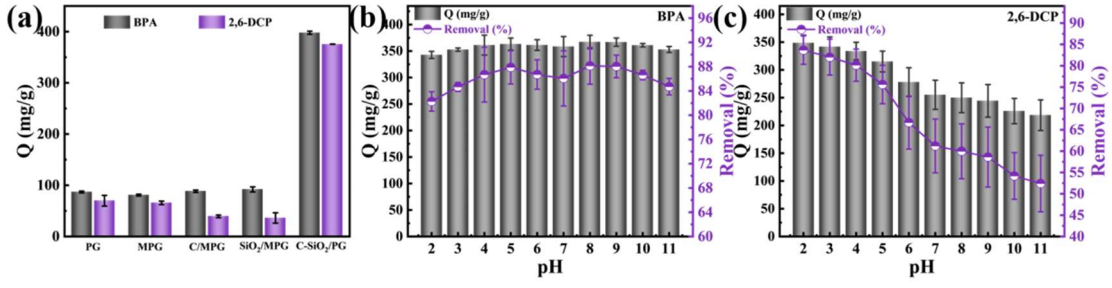

Figure 11. (**a**) Adsorption performance of PG-based adsorbents with different modification methods for BPA and 2,6-DCP; Effect of pH on the adsorption of (**b**) BPA and (**c**) 2,6-DCP by C-SiO_2/MPG.

3.3. Optimization of Adsorption Conditions

3.3.1. Effect of pH on Adsorption

Figure 11b,c shows the variation of the adsorption capacity of BPA and 2,6-DCP on C-SiO_2/MPG with different pH values. The adsorption of BPA on C-SiO_2/MPG is more resistant to pH changes, which is mainly due to the different pKa values of BPA and 2,6-DCP. BPA and 2,6-DCP are both dissociated organic compounds with pKa values of 9.6

(pKa1), 10.2 (pKa2) and 6.79, respectively [36]. As the pH approaches or exceeds their pKa values, BPA and 2,6-DCP gradually dissociate into their anionic forms, leading to a decrease in hydrophobicity [1]. The adsorption of 2,6-DCP is the largest at pH 2, thus, the pH of the BPA solution was not adjusted in subsequent experiments, and the pH of 2,6-DCP adsorption was adjusted to 2.

In a wide pH range (2–11), the entire surface of C-SiO_2/MPG is positively charged. BPA exists as non-ionized molecules at pH < 9.6 and gradually dissociates into monovalent or divalent anion forms at pH > 9.6. The removal ability of C-SiO_2/MPG for BPA in this range is not sensitive to pH changes, which indicates that electrostatic attraction has little effect on the removal of anionic BPA [28]. The hydrophobic interactions and hydrogen bonding between C-SiO_2/MPG and BPA are key factors in maintaining stable adsorption capacity[37]. As shown in Figure 11c, the adsorption of 2,6-DCP by C-SiO_2/MPG under alkaline conditions is inhibited, and the electrostatic promotion effect between positively charged C-SiO_2/MPG and anionic chlorophenol is not obvious in this process. Thus electrostatic interaction is not the mechanism for the removal of 2,6-DCP. The dissociation of 2,6-DCP at higher pH can be the main reason for the decrease in removal efficiency because this reduces hydrogen bonding and hydrophobic interactions to a certain extent [18]. When pH > 6.79, the dissociated anion form dominates the solution compared to the 2,6-DCP molecule. Since the chlorophenol anion is hydrophilic, the hydrophobic interaction between C-SiO_2/MPG and 2,6-DCP molecules will be greatly weakened, thereby reducing the adsorption of 2,6-DCP [38].

3.3.2. Effect of CTAB Addition on Adsorption

The effect of CTAB addition on the adsorption of BPA and 2,6-DCP by C-SiO_2/MPG is shown in Figure 12a. The adsorption performance of C-SiO_2/MPG is the highest when the CTAB addition is 1.5 g. Too low a CTAB amount cannot incorporate enough alkyl chains into C-SiO_2/MPG to enhance its hydrophobicity [6]. Too high a CTAB amount may cause overloading on the surface of C-SiO_2/MPG, resulting in blockage of the pore structure and reducing the effective adsorption area [31].

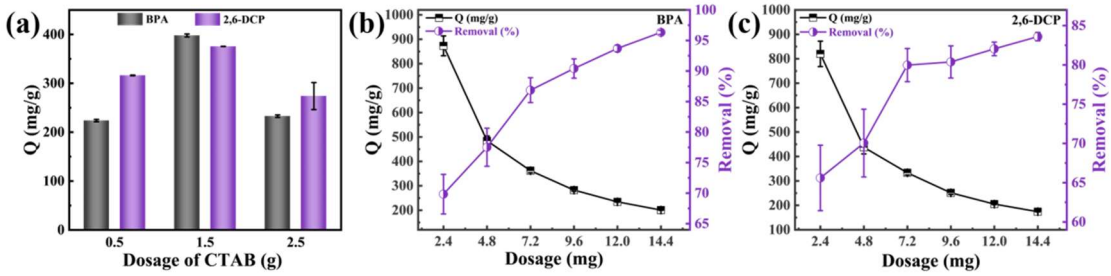

Figure 12. (**a**) Effects of CTAB addition and C-SiO_2/MPG dosage on the adsorption of (**b**) BPA and (**c**) 2,6-DCP.

3.3.3. Effect of Adsorbent Dosage on Adsorption

The experimental study was conducted on 100 mg/L BPA and 2,6-DCP (pH = 2) solutions using different adsorbent dosages, namely 2.4, 4.8, 7.2, 9.6, 12 and 14.4 mg. It can be clearly seen from Figure 12b,c that when the amount of adsorbent increases from 4.8 mg to 7.2 mg, the removal rate of BPA and 2,6-DCP in the solvent increases significantly, but when the amount of adsorbent continues to increase, the removal rate of BPA and 2,6-DCP in the solvent does not increase significantly, and the unit adsorption efficiency decreases. Considering the cost and the higher removal rate of phenolic pollutants, the author chooses the C-SiO_2/MPG amount of 7.2 mg.

3.3.4. Effects of Time and Initial Concentration on Adsorption

Figure 13a,b shows that BPA and 2,6-DCP adsorb rapidly due to the large number of vacant sites available on C-SiO_2/MPG at this starting point [36]. To ensure the saturation or equilibrium of adsorption sites on the C-SiO_2/MPG surface at three concentrations, 90 min was selected as the adsorption equilibrium time.

As can be seen from Figure 13c,d, at three temperatures, increasing the initial concentrations of BPA and 2,6-DCP causes the active sites on the C-SiO_2/MPG surface to be surrounded by more pollutant molecules, resulting in a higher degree of adsorption. Increasing the initial concentrations of BPA and 2,6-DCP molecules can provide the necessary driving force to overcome the mass transfer resistance between the water phase and the solid phase, which is conducive to the transfer of BPA and 2,6-DCP molecules from the water phase to the adsorbent surface [36].

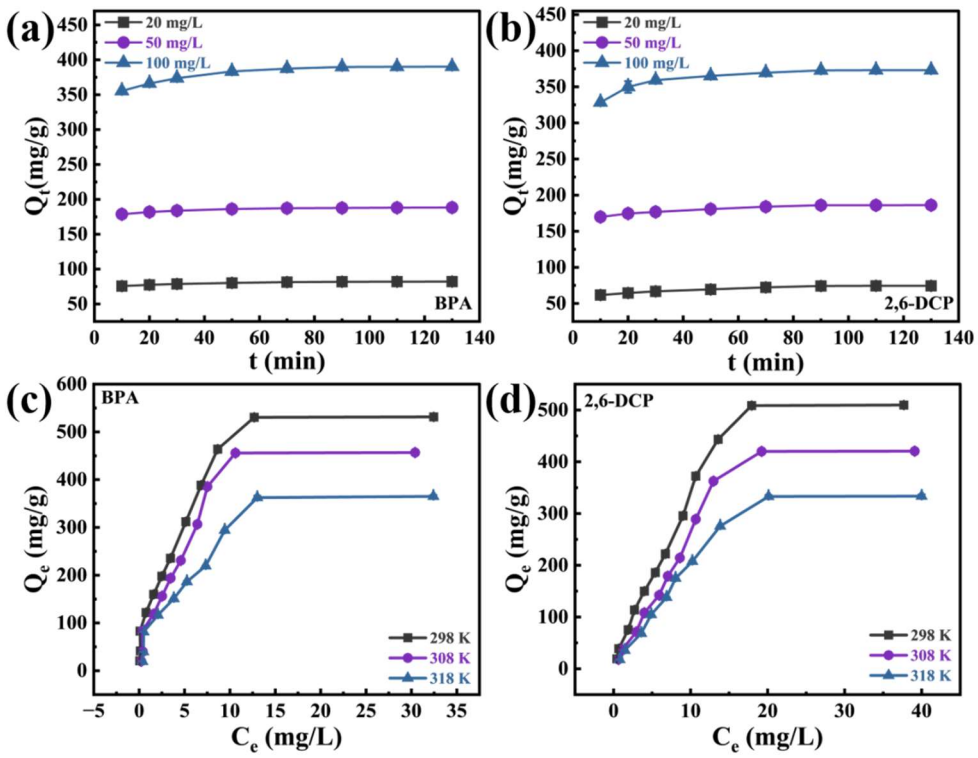

Figure 13. Effects of contact time on the adsorption of (**a**) BPA and (**b**) 2,6-DCP by C-SiO_2/MPG and different initial concentrations on the adsorption of (**c**) BPA and (**d**) 2,6-DCP by C- SiO_2/MPG.

3.4. Adsorption Kinetics Studies

Figure 14 and Table 1 show the kinetic model fitting diagram and kinetic parameters for the adsorption of BPA and 2,6-DCP. Comparing the results of Figure 14a–h and Table 1, the PSO model fits the experimental data with a higher R^2, and the experimental values of the equilibrium adsorption amount at different concentrations are closer to the theoretical values. The PSO model can better describe the adsorption kinetics of BPA and 2,6-DCP, which indicates that chemical adsorption is important in the rate-controlling step. From the results obtained by the IPD model in Table 1, the R^2 values of BPA and 2,6-DCP adsorption are lower than those of the respective PSO models. Therefore, this model is unlikely to be the rate-controlling step for the adsorption of BPA and 2,6-DCP on C-SiO_2/MPG [17]. The results of kinetic data fitting show that the adsorption of BPA and 2,6-DCP by C-SiO_2/MPG is mainly chemical diffusion rather than simple physical diffusion, which means that the adsorption process involves the binding force between the groups in C-SiO_2/MPG and the pollutant molecules [39].

Table 1. Kinetic model parameters for the adsorption of BPA and 2,6-DCP on C-SiO_2/MPG.

	C_0 (mg/L)	$Q_{e,exp}$ (mg/g)	Pseudo-First-Order			Pseudo-First-Order		
			K_1	Q_e (mg/g)	R^2	K_1	Q_e (mg/g)	R^2
BPA	20	82.12	0.018	8.39	0.9593	0.009	82.78	0.9998
	50	188.27	0.003	27.76	0.8181	0.008	188.31	0.9999
	100	390.17	0.010	61.83	0.8413	0.002	389.10	0.9996
2,6-DCP	20	74.42	0.012	24.01	0.9587	0.012	68.73	0.9999
	50	186.04	0.004	48.16	0.9297	0.003	187.62	0.9999
	100	373.02	0.008	92.08	0.8591	0.002	377.36	0.9999
	C_0 (mg/L)	$Q_{e,exp}$ (mg/g)	Intraparticle Diffusion			Elovich		
			K_i	I	R^2	a	b	R^2
BPA	20	82.12	0.762	74.18	0.9466	69.46	2.699	0.9828
	50	188.27	1.086	177.33	0.8895	170.73	3.782	0.9687
	100	390.17	4.779	344.82	0.8995	320.61	15.356	0.9751
2,6-DCP	20	74.42	1.951	55.63	0.9803	50.59	4.693	0.9626
	50	186.04	1.853	166.59	0.9564	153.37	6.934	0.9785
	100	373.02	6.377	311.98	0.8953	284.78	19.565	0.9659

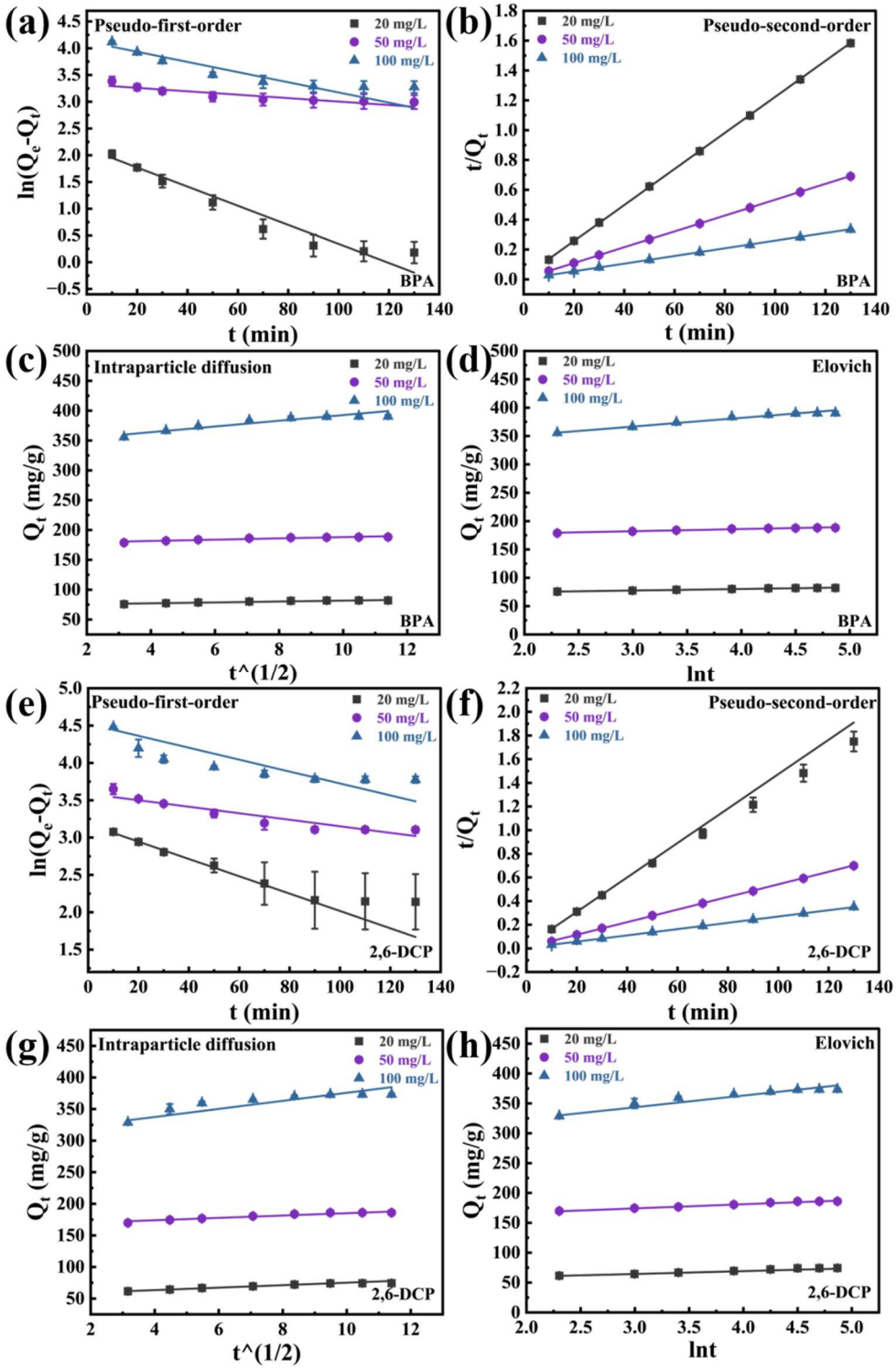

Figure 14. Kinetic fitting curves of (**a**–**d**) BPA and (**e**–**h**) 2,6-DCP adsorption on C-SiO_2/MPG at different times.

3.5. Adsorption Isotherm Studies

The adsorption isotherm study gives the equilibrium relationship of BPA and 2,6-DCP concentrations in the water-solid two-phase at a certain temperature. The fitting curve and the parameters of the corresponding model are shown in Figure 15 and Table 2, respectively. The results show that the Langmuir model can well fit the adsorption data of BPA and 2,6-DCP on C-SiO_2/MPG, indicating that C-SiO_2/MPG is a monolayer adsorption process for BPA and 2,6-DCP, and the energy equivalent adsorption sites on it form the adsorption layer through direct interaction. In addition, the increase in temperature reduces the experimental equilibrium adsorption capacity of BPA and 2,6-DCP, indicating that lower temperatures are conducive to the adsorption of BPA and 2,6-DCP on C-SiO_2/MPG [7]. The saturated adsorption

capacities obtained by fitting the experimental results of BPA and 2,6-DCP with the Langmuir model are 561.79 mg/g and 531.91 mg/g, respectively.

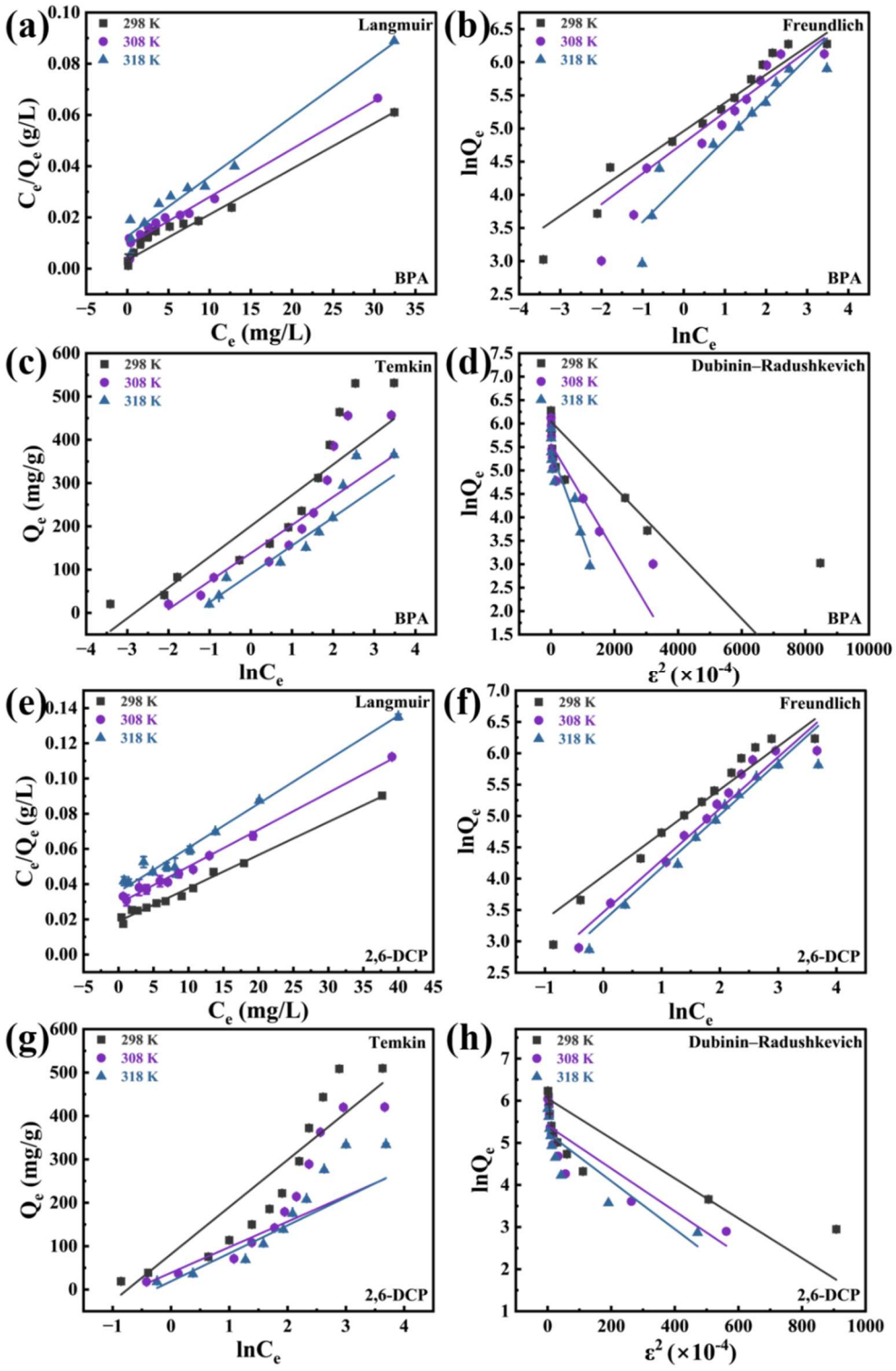

Figure 15. Isotherm model fitting curves of (**a**–**d**) BPA and (**e**–**h**) 2,6-DCP adsorption on C-SiO_2/MPG at different concentrations.

The adsorption amount of BPA is higher than that of 2,6-DCP, which indicates that the hydrophobic C-SiO_2/MPG has a higher affinity for BPA. The magnitude of the affinity is consistent with the solute hydrophobicity determined by the octanol-water partition coefficient. The logarithmic Kow of BPA and 2,6-DCP are 3.3 and 2.90, respectively [38,39]. The logarithmic Kow of hydrophobic aromatic compounds is inversely proportional to the water solubility constant (log K_w). In addition, BPA is a molecule with two phenolic hydroxyl groups, which can produce more hydrogen bonds with C-SiO_2/MPG than 2,6-DCP [26].

Table 2. Various isotherm model parameters for the adsorption of BPA and 2,6-DCP on C-SiO_2/MPG.

Isotherms	Parameters	BPA			2,6-DCP		
		298 K	308 K	318 K	298 K	308 K	318 K
$Q_{m,exp}$ (mg/g)		531.46	456.64	364.90	509.67	420.45	330.37
Langmuir	Q_m (mg/g)	561.79	534.76	429.18	531.91	476.19	400.01
	K_L (L/mg)	0.5329	0.2017	0.1846	0.0996	0.0726	0.0702
	R^2	0.9905	0.9741	0.9674	0.9907	0.9849	0.9831
Freundlich	K_F (L/mg)	142.84	119.60	67.30	56.82	31.99	27.94
	n	2.3465	2.1622	1.6176	1.4491	1.2124	1.8435
	R^2	0.9418	0.9589	0.9563	0.9507	0.9365	0.9595
Temkin	A_T	200.77	138.09	89.91	81.49	38.72	18.94
	B_T	71.051	64.859	65.402	108.66	58.937	64.529
	R^2	0.8609	0.9187	0.9350	0.9193	0.7599	0.8854
Dubinin-Radushkevich	Q_m (mg/g)	421.42	259.06	226.44	424.78	223.02	187.33
	K_D (mol^2/J^2)	7.0121×10^{-8}	1.1420×10^{-7}	1.8489×10^{-7}	4.7394×10^{-7}	5.0757×10^{-7}	5.7039×10^{-7}
	E (J/mol)	2670.3	2092.4	1644.5	1027.1	992.51	936.27
	R^2	0.8304	0.8279	0.9135	0.8967	0.7454	0.7568

The constants n obtained by fitting the BPA and 2,6-DCP adsorption data with the Freundlich model at three temperatures are in the range of 1–10, which shows that C-SiO_2/MPG is a good candidate material for the adsorption of BPA and 2,6-DCP. The Freundlich constant n of BPA adsorption fitted by the Freundlich model at 298 K is higher than that of 2,6-DCP adsorption, indicating that C-SiO_2/MPG exhibits a stronger adsorption effect on BPA than 2,6-DCP [1]. The Temkin isotherm is used as a theoretical model to illustrate that the process involves physical adsorption. The adsorption energy can be evaluated by the D-R parameter. The data in Table 2 show that the adsorption energies of the two organic phenols at three temperatures are all less than 8 kJ/mol, indicating that physical effects such as hydrophobicity and hydrogen bonding contribute to the adsorption of BPA and 2,6-DCP [37].

3.6. Adsorption Thermodynamics Study

Thermodynamic studies provide information on the spontaneity, endothermicity or exothermicity of the adsorption phenomenon and the potential increase or decrease in randomness at the solid/liquid interface, the parameters of which can serve as the basis for explaining the adsorption mechanism. As shown in Figure 16a,c, the increase in temperature leads to a decrease in the adsorption amount and removal rate, which can be explained by the weakening of the interaction between BPA and 2,6-DCP molecules and C-SiO_2/MPG at high temperatures [34].

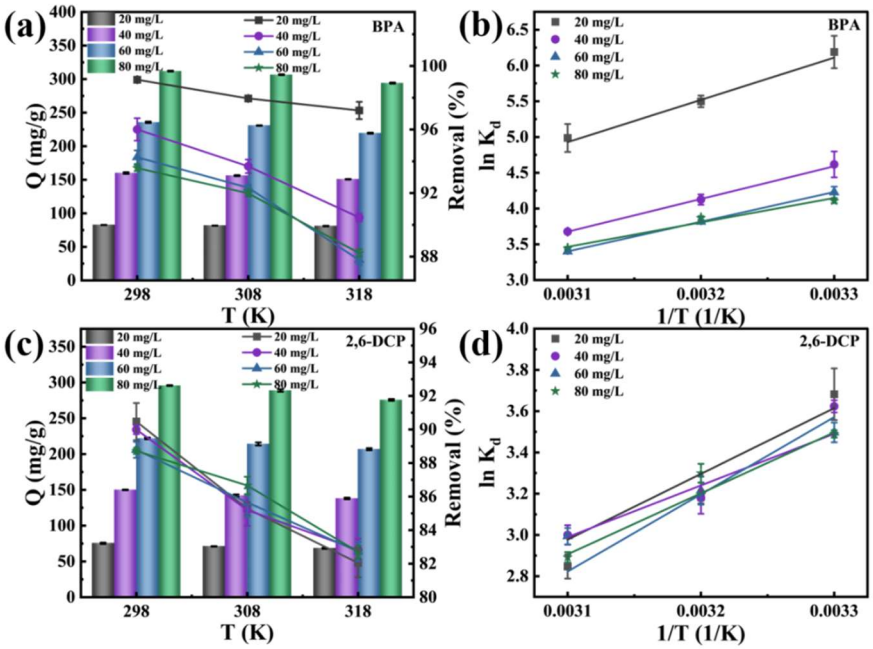

Figure 16. Effect of temperature on the adsorption of (**a**) BPA and (**c**) 2,6-DCP on C-SiO_2/MPG; van't Hoff plots of (**b**) BPA and (**d**) 2,6-DCP adsorption.

Table 3 gives the thermodynamic parameters of the adsorption of BPA and 2,6-DCP on C-SiO_2/MPG. As expected, the negative value of ΔG increases with decreasing temperature, indicating that the adsorption of BPA and 2,6-DCP is easier at lower temperatures [7]. The negative ΔH values under various conditions indicate that the adsorption of BPA and 2,6-DCP on C-SiO_2/MPG is an exothermic process, and the addition of additional heat will reduce the adsorption capacity of both on C-SiO_2/MPG. The negative ΔS value of this process indicates that the adsorption of BPA and 2,6-DCP is associated with a decrease in entropy and randomness[35].

Table 3. Thermodynamic parameters of BPA and 2,6-DCP adsorption on C-SiO_2/MPG.

	C_0 (mg/L)	ΔH (KJ/mol)	ΔS (J/mol/K)	ΔG (KJ/mol)		
				298 K	308 K	318 K
BPA	20	−49.13	−111.34	−15.95	−14.84	−13.73
	40	−38.02	−87.30	−12.01	−11.13	−10.26
	60	−34.54	−78.80	−11.06	−10.27	−9.49
	80	−28.42	−59.29	−10.75	−10.16	−9.56
2,6-DCP	20	−26.50	−57.39	−9.39	−8.82	−8.25
	40	−20.82	−39.73	−8.99	−8.59	−8.19
	60	−28.87	−72.80	−7.12	−6.39	−5.66
	80	−21.57	−51.97	−6.08	−5.56	−5.04

3.7. Comparison of Different Adsorbents

Table 4 shows the comparison of C-SiO_2/MPG with BPA and 2,6-DCP adsorbents reported in the literature based on several factors.

Table 4. Comparison of the adsorption capacity of different adsorbents for BPA and 2,6-DCP.

Adsorbate	Adsorbent	Surface Areas (m^2/g)	Applicable pH	Q_m (mg/g)	Ref.
BPA	CPS-PS	3.78	2–8	270.3	[1]
	PAC/CA/PVA hydrogel	319.83	2–9	64.6	[39]
	AHPN72	2220	7	78	[37]
	HC_{AC}	131.21	2	53.43	[26]
	C-SiO_2/MPG	68.8	2–11	567.79	This work
2,6-DCP	Fe_3O_4@St–DVB	-	2	128.519	[24]
	SWCNT	625	4.8	55.3	[38]
	J-MIPs/cys	-	5	129.4	[18]
	Al-$PILC_{AE}$	277	4	98.46	[36]
	C-SiO_2/MPG	68.8	2	531.91	This work

Compared with the reported adsorbents listed in the table, the adsorption capacity of C-SiO_2/MPG in this study is competitive among these adsorbents. The BET values of other materials mentioned in the table are significantly higher than that of C-SiO_2/MPG, but the maximum adsorption of BPA and 2,6-DCP on C-SiO_2/MPG is relatively high. The prepared C-SiO_2/MPG has stable adsorption performance for BPA at different pH values, and C-SiO_2/MPG can be quickly magnetically separated from the solution under the action of an external magnetic field after adsorbing BPA and 2,6-DCP. The research results show that C-SiO_2/MPG has potential application prospects in the treatment of industrial wastewater containing BPA and 2,6-DCP.

3.8. Effect of Background Electrolyte and Humic Acid

Figure 17a–d shows the effects of anion and cation types and ionic strength on the adsorption of BPA and 2,6-DCP by C-SiO_2/MPG. Negatively charged anions can be adsorbed on the positively charged surface of C-SiO_2/MPG through electrostatic interactions, thereby occupying certain active sites and reducing the removal rate of target pollutants [27]. The experimental results show that except for PO_4^{3-}, inorganic anions have a positive effect on the adsorption of BPA and 2,6-DCP, which can be explained by the increase in ionic strength promoting the occurrence of the "salting-out effect" [10], further enhancing the interaction between C-SiO_2/MPG and BPA and 2,6-DCP. The increase in inorganic cation concentration leads to different degrees of increase in the adsorption of BPA and 2,6-DCP by C-SiO_2/MPG. This enhancement can also be attributed to the salting-out effect that reduces the solubility of BPA and 2,6-DCP in aqueous solution [40].

HA contains aromatic rings and oxygen-containing functional groups (-COOH and Ar-OH), which can occupy the active sites of the adsorbent through π-π interactions, hydrogen bonds, and hydrophobic interactions [27]. Figure 17e,f shows the effect of different concentrations of HA on the adsorption of BPA and 2,6-DCP. The increase in HA concentration leads to a decrease in the adsorption of BPA and 2,6-DCP by C-SiO_2/MPG to varying degrees. On the one hand, it is attributed to the competitive adsorption of HA, and on the other hand, the functional groups such as carboxyl, phenolic and amino groups on the surface of HA combine with BPA and 2,6-DCP in the solution through complexation, increasing their solubility in aqueous solution, thereby reducing adsorption [40].

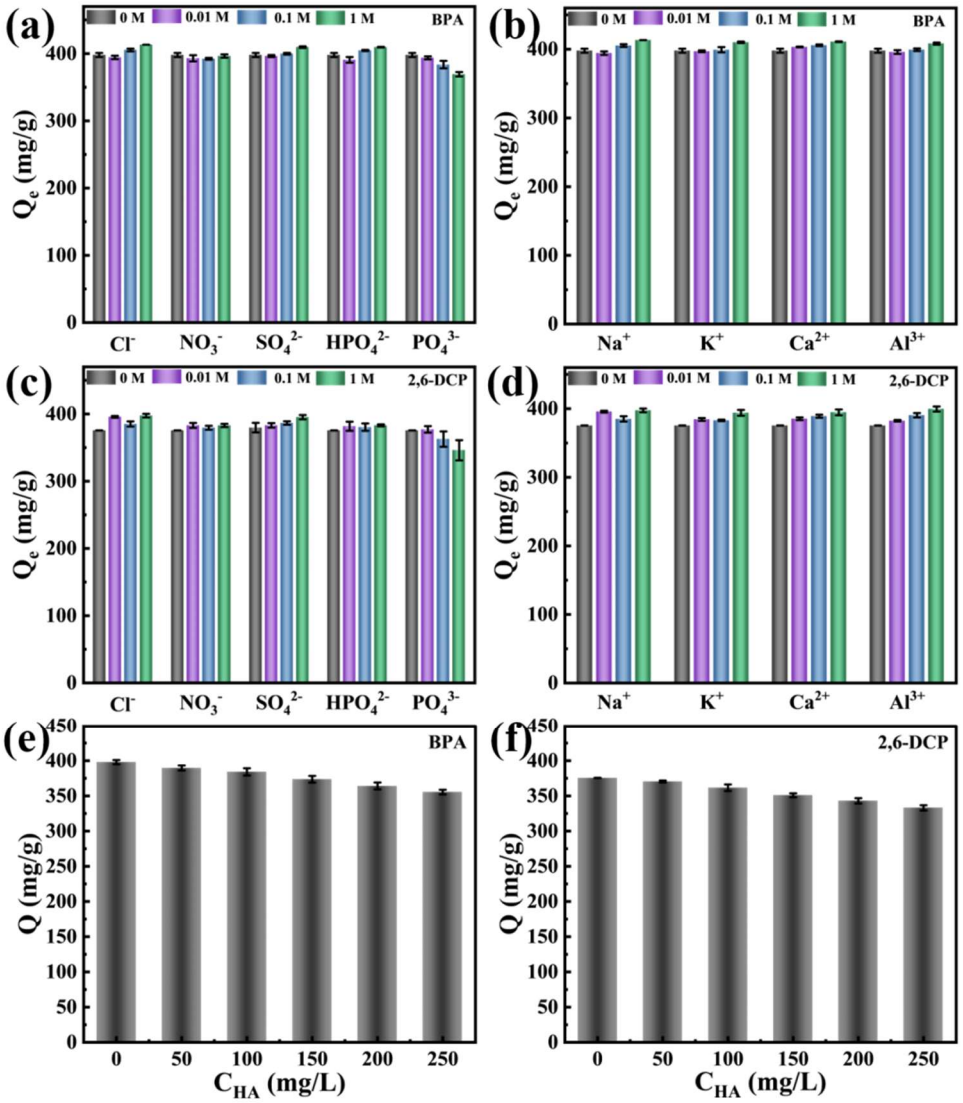

Figure 17. Effects of anionic and cationic electrolytes on the adsorption of (**a**,**b**) BPA and (**c**,**d**) 2,6-DCP on C-SiO_2/MPG; Effects of HA on the adsorption of (**e**) BPA and (**f**) 2,6-DCP.

3.9. Adsorption Performance of C-SiO_2/MPG in Real Water Samples

In order to study the potential of the prepared C-SiO_2/MPG to remove BPA and 2,6-DCP in real water samples, it was applied to three water samples: DIW, TP and RW. The results of Figure 18a,b show that the adsorption capacity of C-SiO_2/MPG for BPA and 2,6-DCP in different water samples has no significant decrease, indicating that the hydrophobic magnetic material is suitable for the removal of phenolic compounds in water.

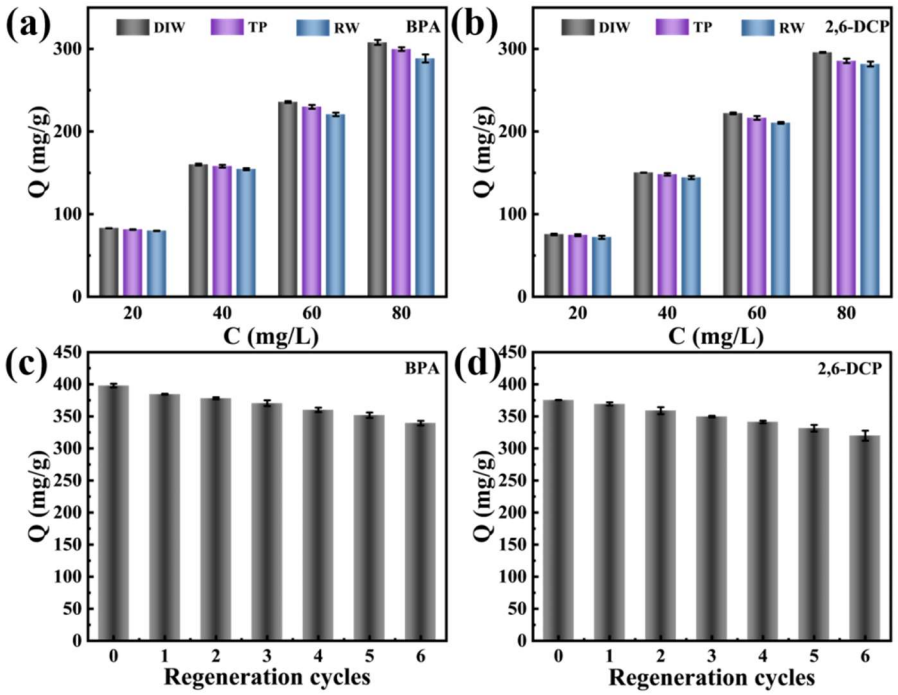

Figure 18. Adsorption performance of C-SiO_2/MPG for (**a**) BPA and (**b**) 2,6-DCP in real water samples; regeneration experiment after C-SiO_2/MPG adsorbs (**c**) BPA and (**d**) 2,6-DCP.

3.10. Regeneration of C-SiO_2/MPG

The spent C-SiO_2/MPG was regenerated by washing with ethanol and subjected to six consecutive cycles of BPA and 2,6-DCP adsorption-desorption, as shown in Figure 18c,d. The adsorption capacity of C-SiO_2/MPG for BPA and 2,6-DCP slightly decreased after the first cycle. The loss of adsorption capacity after each cycle can be attributed to incomplete desorption of BPA and 2,6-DCP, pore blockage, and the loss of active functional sites on the adsorbent needed for hydrogen bonding.After six cycles, the adsorption of BPA and 2,6-DCP by C-SiO_2/MPG decreased from 397.92 mg/g and 375.46 mg/g to 339.36 mg/g and 319.86 mg/g, which is equivalent to a decrease in removal efficiency of 14.6% and 14.8%, respectively. The results showed that C-SiO_2/MPG is regenerable and has the potential for reuse in treating wastewater containing BPA and 2,6-DCP.

3.11. Adsorption Mechanism of C-SiO_2/MPG

The FT-IR and XPS results mentioned above indicate that hydrophobic and hydrogen bonding interactions play a key role in the adsorption of BPA and 2,6-DCP. Adsorption experiments under a wide range of pH conditions showed that C-SiO_2/MPG exhibited good adsorption of molecular BPA and 2,6-DCP under acidic and neutral conditions. According to the difference in zeta potential and the adsorption capacity of the two phenols, it can be verified that there is almost no electrostatic attraction between C-SiO_2/MPG and the pollutants. The CTAB micelles formed on the surface of C-SiO_2/MPG further enhance the adsorption capacity of hydrophobic C-SiO_2/MPG for hydrophobic BPA and 2,6-DCP [10]. The hydrogen bonds in the adsorption process exist between the oxygen-containing functional groups and amino N atoms on the surface of C-SiO_2/MPG and the -OH of BPA and 2,6-DCP molecules. Based on the results of FT-IR, XPS and pH studies, the potential mechanism of enhanced adsorption of BPA and 2,6-DCP by C-SiO_2/MPG was proposed, which is mainly achieved through two pathways: hydrophobic interaction and hydrogen bonding, as shown in Figure 19.

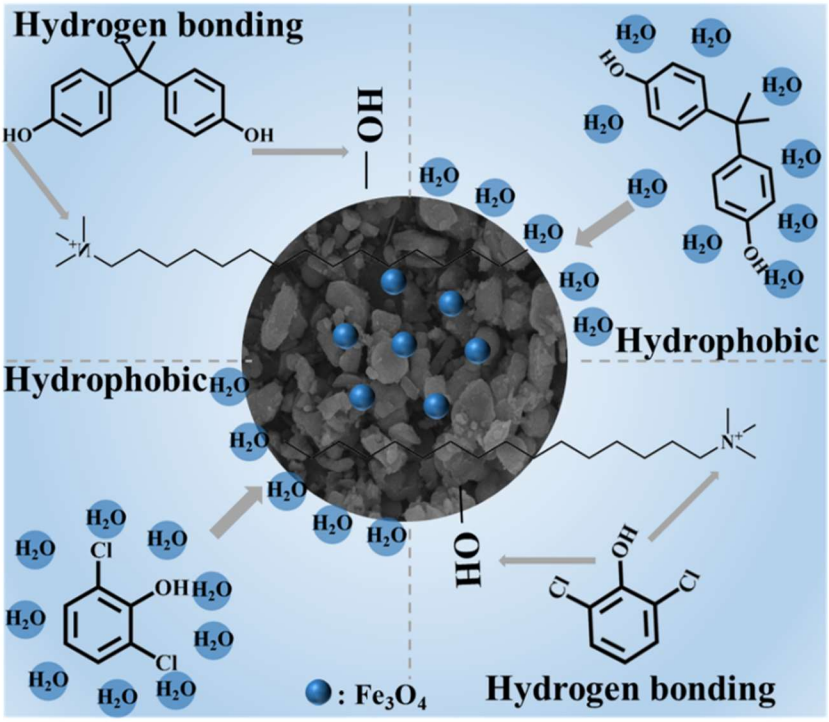

Figure 19. Schematic diagram of the adsorption mechanism of BPA and 2,6-DCP on the hydrophobic magnetic composite C-SiO_2/MPG.

4. Conclusions

In this study, a new hydrophobic magnetic C-SiO_2/MPG composite material was prepared using co-precipitation and sol-gel methods. It was used for the adsorption of BPA and 2,6-DCP. This method combines the advantages of magnetic nanoparticles and hydrophobic alkyl chains as adsorbents, making the adsorbent easy to recover from the sample matrix magnetically. The PSO kinetic model and Langmuir isotherm model fit well on the adsorption of BPA and 2,6-DCP, indicating that the monolayer chemical adsorption has a rate-controlling step. The Langmuir equation fitting calculation shows that the maximum adsorption capacity of C-SiO_2/MPG for BPA and 2,6-DCP at 298 K is 561.79 mg/g and 531.91 mg/g, respectively. The results of adsorption thermodynamics indicate that the adsorption of BPA and 2,6-DCP on C-SiO_2/MPG is spontaneous, accompanied by the process of entropy reduction. C-SiO_2/MPG showed good adsorption performance for BPA and 2,6-DCP in coexisting ions, HA, real water samples and regeneration experiments, proving that it can be used to treat phenolic wastewater. In addition, the results of FT-IR, XPS and pH studies showed that hydrogen bonding and hydrophobic interactions are the potential mechanisms for the enhanced adsorption of BPA and 2,6-DCP. This study will broaden the resource utilization of industrial waste PG and provide a reference for the design of efficient BPA and 2,6-DCP adsorbents.

Acknowledgments

Financial support from Hubei Three Gorges Laboratory through grant No. SK211007 is acknowledged.

Author Contributions

Conceptualization, Q.Z. and D.L.; Methodology, M.L. and J.J.; Validation, M.L. and J.J.; Formal Analysis, R.C., J.Y., M.L. and D.L.; Investigation, M.L. and J.J.; Writing—Original Draft Preparation, J.J.; Writing—Review & Editing, Q.Z.; Supervision, D.L. and Q.Z.

Ethics Statement

Not applicable.

Informed Consent Statement

Not applicable.

Funding

This study is supported by Hubei Three Gorges Laboratory through grant No. SK211007, the Joint Funds of the National Natural Science Foundation of China (U24A2094), the Joint Funds for Innovation and Development of Natural Science Foundation of Hubei Province (2024AFD138) and the Open and Innovation Fund of Hubei Three Gorges Laboratory (SK240009).

Declaration of Competing Interest

The authors declare that they have no known competing financial interests or personal relationships that could have appeared to influence the work reported in this paper.

References

1. Wang H, Tian T, Wang D, Xu F, Ren W. Adsorption of bisphenol A and 2,4-dichlorophenol onto cetylpyridinium chloride-modified pine sawdust: A kinetic and thermodynamic study. *Environ. Sci. Pollut. Res.* **2022**, *29*, 18932–18943.
2. National Research Council, Commission on Life Sciences, Board on Environmental Studies, Committee on Hormonally Active Agents in the Environment. *Hormonally Active Agents in the Environment*; National Academies Press: Washington, DC, USA, 2000.
3. Cardona Y, Węgrzyn A, Miśkowiec P, Korili SA, Gil A. Catalytic photodegradation of organic compounds using TiO_2/pillared clays synthesized using a nonconventional aluminum source. *Chem. Eng. J.* **2022**, *446*, 136908.
4. Yelatontsev D. Utilization of phosphogypsum in phenol removal from coking wastewater. *J. Hazard. Mater. Lett.* **2023**, *4*, 100089.
5. Igwegbe CA, Al-Rawajfeh AE, Al-Itawi H, Sharadqah S, Al-Qazaqi S, Abu Hashish E, et al. Utilization of calcined gypsum in water and wastewater treatment: Removal of phenol. *J. Ecol. Eng.* **2019**, *20*, 1–10.
6. Salehinia S, Ghoreishi SM, Maya F, Cerdà V. Hydrophobic magnetic montmorillonite composite material for the efficient adsorption and microextraction of bisphenol A from water samples. *J. Environ. Chem. Eng.* **2016**, *4*, 4062–4071.
7. Geng P, Hao H, Guo J, Wang Y, Ma J, Wang X, et al. One-Step Fabrication of Magnetic Polymer/Montmorillonite Adsorbent for Highly Efficient Phenol Adsorption. *Clays Clay Miner.* **2023**, *71*, 377–396.
8. Bhatnagar A, Anastopoulos I. Adsorptive removal of bisphenol A (BPA) from aqueous solution: A review. *Chemosphere* **2017**, *168*, 885–902.
9. Zhang Y, Liu C, Luo L, Shi Y, Chen Y, Wang S, et al. One-step hydrothermal synthesis of CTAB-modified SiO_2 for removal of bisphenol A. *Water Sci. Technol.* **2017**, *76*, 928–938.
10. Wang L-C, Ni X-j, Cao Y-H, Cao G-q. Adsorption behavior of bisphenol A on CTAB-modified graphite. *Appl. Surf. Sci.* **2018**, *428*, 165–170.
11. Hoshyar SA, Barzani HA, Yardım Y, Şentürk Z. The effect of CTAB, a cationic surfactant, on the adsorption ability of the boron-doped diamond electrode: Application for voltammetric sensing of Bisphenol A and Hydroquinone in water samples. *Colloids Surf. A Physicochem. Eng. Asp.* **2021**, *610*, 125916.
12. Meneses IP, Novaes SD, Dezotti RS, Oliveira PV, Petri DFS. CTAB-modified carboxymethyl cellulose/bagasse cryogels for the efficient removal of bisphenol A, methylene blue and Cr (VI) ions: Batch and column adsorption studies. *J. Hazard. Mater.* **2022**, *421*, 126804.
13. Rottman C, Grader G, De Hazan Y, Melchior S, Avnir D. Surfactant-induced modification of dopants reactivity in sol− gel matrixes. *J. Am. Chem. Soc.* **1999**, *121*, 8533–8543.
14. Addy M, Losey B, Mohseni R, Zlotnikov E, Vasiliev A. Adsorption of heavy metal ions on mesoporous silica-modified montmorillonite containing a grafted chelate ligand. *Appl. Clay Sci.* **2012**, *59*, 115–120.
15. Wang P, Wang X, Yu S, Zou Y, Wang J, Chen Z, et al. Silica coated Fe_3O_4 magnetic nanospheres for high removal of organic pollutants from wastewater. *Chem. Eng. J.* **2016**, *306*, 280–288.
16. AbdulRazak AA, Shakor ZM, Rohani S. Optimizing Biebrich Scarlet removal from water by magnetic zeolite 13X using response surface method. *J. Environ. Chem. Eng.* **2018**, *6*, 6175–6183.
17. Ahsan MA, Islam MT, Hernandez C, Kim H, Lin Y, Curry ML, et al. Adsorptive removal of sulfamethoxazole and bisphenol A from contaminated water using functionalized carbonaceous material derived from tea leaves. *J. Environ. Chem. Eng.* **2018**, *6*, 4215–4225.
18. Liu J, Wang P, Zhou M, Ma Y, Niu X, Pan G, et al. Tailored Janus silica nanosheets integrating bispecific artificial receptors for simultaneous adsorption of 2, 6-dichlorophenol and Pb (ii). *J. Mater. Chem. A* **2019**, *7*, 16161–16175.
19. Wang W-S, Xu H-Y, Li B, Dai L-Y, Zhang S-Q, Xu Y, et al. Preparation, catalytic efficiency and mechanism of Fe_3O_4/HNTs heterogeneous Fenton-like catalyst. *Mater. Today Commun.* **2023**, *36*, 106821.
20. Li M, Liu H, Chen T, Dong C, Sun Y. Synthesis of magnetic biochar composites for enhanced uranium (VI) adsorption. *Sci. Total Environ.* **2019**, *651*, 1020–1028.

21. Cui J, Liu T, Zhang Q, Wang T, Hou X. Rapid microwave synthesis of Fe_3O_4-PVP@ ZIF-67 as highly effective peroxymonosulfate catalyst for degradation of bisphenol F and its mechanism analysis. *Chem. Eng. J.* **2021**, *404*, 126453.
22. Yi Z, Jiang T, Cheng Y, Tang Q. Effect of SiO_2 aerogels loading on photocatalytic degradation of nitrobenzene using composites with tetrapod-like ZnO. *Nanotechnol. Rev.* **2020**, *9*, 1009–1016.
23. Ardani M, Imani M, Tadjarodi A. Core shell Fe_3O_4@ TiO_2/silica aerogel nanocomposite; synthesis and study of structural, magnetic and photocatalytic properties. *Microporous Mesoporous Mater.* **2022**, *338*, 111757.
24. Yu P, Sun Q, Pan J, Tan Z, Dai J, Yan Y, et al. Performance of Poly (Styrene—Divinylbenzene) Magnetic Porous Microspheres Prepared by Suspension Polymerization for the Adsorption of 2,4-Dichlorophenol and 2,6-Dichlorophenol from Aqueous Solutions. *Adsorpt. Sci. Technol.* **2013**, *31*, 641–656.
25. Nguyen-Thi N-T, Pham Tran LP, Le NTT, Cao M-T, Tran T-N, Nguyen NT, et al. The engineering of porous silica and hollow silica nanoparticles to enhance drug-loading capacity. *Processes* **2019**, *7*, 805.
26. Chandrasekar R, Rajendran HK, Narayanasamy S. Valorization of sawdust by mineral acid assisted hydrothermal carbonization for the adsorptive removal of bisphenol A: A greener approach. *Chemosphere* **2022**, *303*, 135171.
27. Ou H, Zhang W, Yang X, Cheng Q, Liao G, Xia H, et al. One-pot synthesis of gC_3N_4-doped amine-rich porous organic polymer for chlorophenol removal. *Environ. Sci. Nano* **2018**, *5*, 169–182.
28. Liang G, Wang Z, Yang X, Qin T, Xie X, Zhao J, et al. Efficient removal of oxytetracycline from aqueous solution using magnetic montmorillonite-biochar composite prepared by one step pyrolysis. *Sci. Total Environ.* **2019**, *695*, 133800.
29. Balkaya N, Cesur H. Adsorption of cadmium from aqueous solution by phosphogypsum. *Chem. Eng. J.* **2008**, *140*, 247–254.
30. Zhao L, Zhang Q, Li X, Ye J, Chen J. Adsorption of Cu (II) by phosphogypsum modified with sodium dodecyl benzene sulfonate. *J. Hazard. Mater.* **2020**, *387*, 121808.
31. Chen G, Liu J, Liu R. Preparation and wave-absorbing properties of low-cost Fe_3O_4/corn straw core composite material. *J. Mater. Sci. Mater. Electron.* **2023**, *34*, 808.
32. Akti F, Balci S. Silica xerogel and iron doped silica xerogel synthesis in presence of drying control chemical additives. *Mater. Chem. Phys.* **2023**, *297*, 127347.
33. Guo Y, Guo S, Ren J, Zhai Y, Dong S, Wang E. Cyclodextrin functionalized graphene nanosheets with high supramolecular recognition capability: Synthesis and host−guest inclusion for enhanced electrochemical performance. *ACS Nano* **2010**, *4*, 4001–4010.
34. Fu X, Sarker S, Ma W, Zhao W, Rong Y, Liu Q. Novel phenylalanine-modified magnetic ferroferric oxide nanoparticles for ciprofloxacin removal from aqueous solution. *J. Colloid Interface Sci.* **2023**, *632*, 345–356.
35. Liu Z, Zhang J, Mou R. Phosphogypsum-Modified Vinasse Shell Biochar as a Novel Low-Cost Material for High-Efficiency Fluoride Removal. *Molecules* **2023**, *28*, 7617.
36. Cardona Y, Korili SA, Gil A. A nonconventional aluminum source in the production of alumina-pillared clays for the removal of organic pollutants by adsorption. *Chem. Eng. J.* **2021**, *425*, 130708.
37. de Lima HHC, Llop MEG, dos Santos Maniezzo R, Moisés MP, Janeiro V, Arroyo PA, et al. Enhanced removal of bisphenol A using pine-fruit shell-derived hydrochars: Adsorption mechanisms and reusability. *J. Hazard. Mater.* **2021**, *416*, 126167.
38. Ding H, Li X, Wang J, Zhang X, Chen C. Adsorption of chlorophenols from aqueous solutions by pristine and surface functionalized single-walled carbon nanotubes. *J. Environ. Sci.* **2016**, *43*, 187–198.
39. Zhou A, Wu X, Chen W, Liao L, Xie P. Fabrication of hydrophobic/hydrophilic bifunctional adsorbent for the removal of sulfamethoxazole and bisphenol A in Water. *J. Environ. Chem. Eng.* **2020**, *8*, 104161.
40. Zhou Y, Cheng G, Chen K, Lu J, Lei J, Pu S. Adsorptive removal of bisphenol A, chloroxylenol, and carbamazepine from water using a novel β-cyclodextrin polymer. *Ecotoxicol. Environ. Saf.* **2019**, *170*, 278–285.